RSC Advances

RSC Advances

ARTICLE

Porous silicon nanoparticles as a nanophotocathode for photoelectrochemical water splitting

Soundarrajan Chandrasekaran,[a] Steven J. P. McInnes,[a] Thomas J. Macdonald,[b] Thomas Nann*[b] and Nicolas H. Voelcker*[a]

The antireflective properties and nanometer size of silicon nanoparticles can be exploited for improving solar energy conversion. We report on using porous silicon nanoparticles as a photocathode for photoelectrochemical water splitting. An enhancement in photocurrent density was observed when porous silicon nanoparticles were decorated with indium phosphide nanocrystals and a bio-inspired iron sulfur carbonyl electrocatalyst. Our system gave a photocurrent density of -2.2 $\mu A/cm^2$, while generating hydrogen gas.

Introduction

The generation of hydrogen (H_2) through solar water electrolysis provides a clean and renewable source of energy.[1-4] Photocatalytic and photoelectrochemical (PEC) water splitting are two ways of producing H_2 from sunlight.[1] For example, photocatalysts can absorb sunlight (of the appropriate energy) and split water molecules into H_2 and oxygen (O_2) when freely suspended in water.[2, 3, 5-8] Silicon, with a band-gap of 1.12 eV is considered to be one of the most suitable materials used in photovoltaic devices, especially when compared to titanium dioxide (band gap 3.0 eV), nickel oxide (3.6 eV) cadmium selenides (band gap 1.7 eV) and cadmium sulphide (band gap 2.4 eV).[9-12] Albeit silicon possesses low band-gap energy, by itself it is not sufficient to split water, which is why tandem-structures, such as semiconductor nanocrystals (NCs), are necessary. Bulk and nanostructured silicon materials in the form of planar silicon,[13, 14] porous silicon (pSi)[15, 16] and silicon nanowires (Si NWs)[17-19] have been widely used for water splitting. Over the years, pSi nanoparticles (NPs) have been used as photoactive materials for chemical/photo-chemical H_2 evolution.[20-24] During the water splitting process, silicon hydride (Si-H) terminated pSi NPs oxidise to silica while reducing the protons to H_2 in the electrolyte solution.[20-24]

Previous reports show 10 nm sized pSi NPs synthesised using CO_2 laser pyrolysis,[20] achieve 100 times faster H_2 production (gH_2 s^{-1} g^{-1} silicon) than electrochemically etched pSi NPs of approximately 3-10 nm,[21] 8-20 nm[22] and 75 nm commercially purchased porous silicon NPs.[23] However, recent research into H_2 production was demonstrated from mesoporous silicon

microparticles of approximately 5-20 µm, synthesised by reducing silicon halogenide.[24] The authors claimed that the high surface area of those mesoporous silicon microparticles significantly improved the H_2 generation. It was found that the H_2 production (gH_2 s^{-1} g^{-1} silicon) was 30 times more efficient for mesoporous silicon microparticles than for the pSi NPs synthesised using the CO_2 laser pyrolysis technique.

PEC cells work by breaking down water molecules into O_2 and H_2 at the photoanode (n-type) and photocathode (p-type), respectively.[4,20] In addition, catalysts can increase the H_2 evolution reaction when fabricated with photoelectrodes. There has only been one previous report of PEC water splitting based on the synthesis of n-type pSi NPs using magnesiothermic reduction of silica.[25] To our knowledge, p-type pSi NPs have not been investigated for PEC water splitting. It is known that the inclusion of indium phosphide (InP) NCs and an iron sulfur carbonyl ($Fe_2S_2(CO)_6$) electrocatalyst on a silicon electrode improves PEC efficiency.[15, 26, 27] In this work, we report a facile strategy to fabricate a PEC water-splitting electrode from p-type pSi NPs, obtained from electrochemical etching, coated with InP NCs and $Fe_2S_2(CO)_6$ catalyst. This is the first example of a pSi NP system sensitised with inorganic nanomaterials as a photocathode for H_2 production.

Experimental

Materials

pSi NPs were produced from p-type silicon wafers (Czochralski, Siltronix Ltd.) with resistivity of 0.8-12 mΩ cm, orientation (100). Hydrofluoric acid (HF) (48%) was purchased from Scharlau Chemie (Chem-Supply Pty. Ltd. Australian representation).

pSi NPs Preparation

pSi NPs are produced via electrochemical anodisation of p-type silicon in a 3:1 mixture of aqueous (48%) HF and ethanol in an 18 cm^2 Teflon cell with a platinum (Pt) counter electrode. A square

[a.] Mawson Institute, University of South Australia, Mawson Lakes Blvd, Adelaide, SA 5095, Australia. Email: Nico.Voelcker@unisa.edu.au
[b.] Ian Wark Research Institute, University of South Australia, Mawson Lakes Blvd, Adelaide, SA 5095, Australia. Email: Thomas.Nann@unisa.edu.au

waveform consisting of a 50 mA/cm^2 lower etch current, applied for 7.3 s, was followed by an upper perforate current of 400 mA/cm^2, and applied for 0.3 s. This square waveform was continued for 474 repeats (approximately 1 h) after which the HF solution was changed to a 1:20 HF:ethanol mixture and a 4 mA/cm^2 constant current was applied for 250 s to electropolish the pSi film into a free standing membrane. The freestanding pSi film was fractured into pSi NPs by ultra-sonication for 16 h in ethanol purged with N$_2$. The resulting NPs solution was spun at 10,000 × g to pellet large particles and the supernatant was filtered through a 200 nm filter membrane and then centrifuged at 22000 × g. The resulting pellet of pSi NPs was re-dispersed in ethanol.

Surface Functionalisation of pSi NPs

The surface functionalisation was achieved by thermally hydrosilylating the pSi NPs in a 1 M toluene solution of allyl mercaptan (AM) at 50 ^{o}C for 15 h. The AM hydrosilylated pSi NPs were purified by washing with toluene (three times), vacuum dried and stored in a glove box.[28]

InP NC Synthesis

InP NCs were synthesised via a slightly modified procedure from Xu et al.[29, 30] In a typical synthesis, indium (III) chloride (0.1 mmol), stearic acid (0.1 mmol), zinc undecylenate (0.2 mmol), and hexadecylamine (0.2 mmol) were added to a Schlenk flask. The mixture was initially purged with N$_2$ before 1-octadecene (~2 ml) was added. The mixture was then vacuum/back filled with N$_2$ before heating to 270 ^{o}C. Upon reaching 270 ^{o}C, a solution of tris(trimethylsilyl)phosphine (1 ml, 0.1 M) in 1-octadecene was rapidly injected causing the temperature of the solution to drop to 250 ^{o}C. The NCs were grown for 10 min at 250 ^{o}C forming a deep red solution. The NCs was cooled to room temperature before being washed twice with ethanol (2 × 60 ml) to remove any excess ligands. The NCs were finally re-dispersed in toluene (10 ml).

Electrode Fabrication

The AM hydrosilylated pSi NPs were sonicated for 1 h in toluene prior to fabrication of the electrodes. To fabricate the electrodes, 100 µl of a 1 mg/ml solution of AM hydrosilylated pSi NPs in toluene was added to a gold-coated glass slide via drop casting in a glove box under Argon. After the NPs were dried, this deposition process was repeated 5 times. The surface was then gently washed with distilled water to removing any unbound pSi NPs. Following this, 5 layers of InP NCs were added to the surface via drop casting. Finally, the InP NCs sensitised electrode was gently washed with distilled water to remove the unbound InP NCs and a final layer of Fe$_2$S$_2$(CO)$_6$ catalyst (in toluene) was drop-casted on the surface.

Surface Characterisation

Scanning electron microscopy (SEM) images and energy-dispersive X-ray (EDX) spectra were obtained on a FEI Quanta 450 environmental SEM. Fourier transform infrared spectra (FTIR) spectra were obtained using a Bruker Hyperion 1000 IR microscope operating with a Bruker Vertex 80 IR spectrometer. The IR microscope was equipped with a liquid nitrogen cooled MCT detector. The spectra were collected over 64 scans, with a resolution of 4 cm^{-1}. All spectra were recorded and analysed using OPUS version 7.0 software, in the range of 650 - 4000 cm^{-1}. Fluorescence microscopy images were recorded with a Nikon Eclipse 50i fluorescence microscope and analysed by NIS Elements software.

Photocurrent and Gas Chromatography Measurements

Samples were irradiated using an Abet solar simulator (air mass 1.5-1 sun) and calibrated against a silicon solar cell (New-Spec). Electrochemical measurements were carried out using a PG 310 potentiostat from HEKA Electronics (Germany). Electrolysis was performed using a sealed three-electrode Teflon photoelectrochemical cell consisting of a Pt counter electrode, a Ag | AgCl 3M KCl reference electrode and the working electrode. The working electrode was illuminated with a light intensity of 100 mW/cm^2 under air mass 1.5 conditions with short 12 s dark and 12 s light cycle to measure the photocurrents for 60 s. The potential between the working and reference electrodes was adjusted between 0 and -500 mV in 100 mV steps. The 1 h run photocurrents were measured under a light cycle at a bias voltage of -400 mV with respect to the open circuit potentials (OCPs). The sample gas in the headspace (310 µl) above the electrolyte was sampled after 1 h and analysed using a SRI 310C series gas chromatograph (GC) with a thermal conductivity detector and a column held at 70 ^{o}C with N$_2$ as the carrier gas.

Results and discussion

pSi NPs

pSi NPs synthesised by CO$_2$ laser pyrolysis[20] and mesoporous silicon microparticles synthesised by reducing silicon halogenide[24] have previously shown efficient H$_2$ production. These synthesis techniques use silane and silicon halogenide as a starting material to synthesise un-doped pSi NPs and then require a further complex doping process before they can be used as a photocathode material for PEC water splitting. Therefore, we chose to fabricate p-type pSi NPs via straightforward electrochemical anodisation technique. pSi films were fabricated using a square waveform to generate alternating layers of high and low porosity. The highly porous layers are weak and disintegrate rapidly during sonication.[11] Fig. S1 shows the top view (A) and cross-sectional (B) SEM images of the pSi film with an average pore size of ~ 13 nm and thickness of ~ 118 µm. The thickness of the each low porosity layer is ~ 240 nm. The pSi membrane was electropolished and removed from the crystalline silicon substrate, which was subjected to sonication for 16 h in ethanol and purged with N$_2$ gas in order to fracture the film into pSi NPs. Fig. 1 shows the SEM image of mesoporous pSi NPs. The inset shows a high-resolution image of the pSi NPs. The average particle size was found to be 161 ± 58 nm with pore sizes of ~ 13 nm.
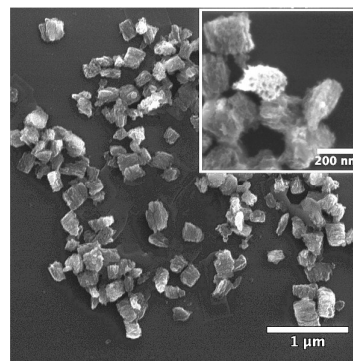

Fig. 1 SEM image of electrochemically anodised pSi NPs. The inset represents the pSi NPs at a higher magnification.

Fig. 2 shows FTIR of freshly prepared pSi NPs (a) and AM hydrosilylated pSi NPs (b). Spectrum (a) shows the Si-Hx stretching peak at 2100 cm^{-1} for the bare pSi NPs.[31] While spectrum (b) also shows Si-Hx stretching, C-H stretching vibrations at 2900 cm^{-1} can now be seen which confirms hydrosilylation of the pSi NPs surface.[32] The peak at 1100 cm^{-1} may be attributed to surface oxidation from Si-O-Si groups, after AM hydrosilylation on pSi NPs when compared to the bare pSi NPs. The AM hydrosilylation imparts the pSi NPs with free thiol end groups, providing anchors for attachment to gold surfaces.[28, 32, 33] The inset shows the corresponding fluorescence images of pSi NPs and AM hydrosilylated pSi NPs after reaction with fluorescein-5-maleimide dye (498 nm excitation) in PBS buffer at pH 7. The green fluorescence of AM hydrosilylated pSi NPs after reaction with the dye confirms the availability of thiol groups on the particle surface.[28]
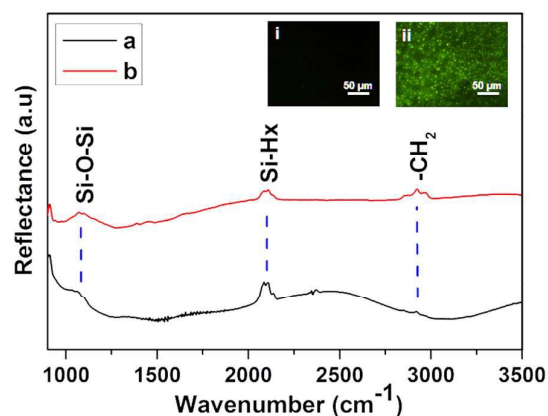

Fig. 2 FTIR spectra of the pSi NPs before (a) and after AM hydrosilylation (b). The inset shows the fluorescence images (FITC filter) of pSi NPs (i) and AM hydrosilylated pSi NPs (ii) after reaction with fluorescein-5-maleimide.

PEC Electrode Performance and GC Measurements

Fig. S2A-B show the top-view SEM images of mesoporous AM hydrosilylated pSi NPs and AM hydrosilylated pSi NPs coated with InP NCs and $Fe_2S_2(CO)_6$ catalyst on gold, respectively. The pores of AM hydrosilylated pSi NPs were covered with InP NCs and $Fe_2S_2(CO)_6$ catalyst coating which is evident from Fig. S2B. Fig. S2C-D show the cross-sectional SEM images corresponding to Fig. S2A-B. The thickness of the layer was measured to be 204 ± 33 nm and 212 ± 21 nm for the AM hydrosilylated pSi NPs (Fig. S2C) and AM hydrosilylated pSi NPs (Fig. S2D) coated with InP NCs and $Fe_2S_2(CO)_6$ catalyst on gold, respectively. The presence of C, O, Fe, Si, Au, S, P and In signals in the EDX spectra confirmed the coating of InP NCs and $Fe_2S_2(CO)_6$ catalyst on the AM hydrosilylated pSi NPs fabricated on gold (Fig. S2E-F). PEC water splitting was carried out in a sealed three-electrode set up with 0.1 M sulfuric acid (H_2SO_4) as the electrolyte. H_2SO_4 was chosen as the electrolyte as it possesses a slightly acidic pH, which helps in improving the electron conduction and contributes more protons for H_2 generation.[34] A solar simulator provided an artificial sunlight (air mass 1.5 irradiation). Table 1 shows the photocurrent density measurements and corresponding OCPs for the fabricated pSi NPs electrodes. The average photocurrent density measurements for the electrode with AM hydrosilylated pSi NPs alone was ~ -300 nA/cm^2, while the hybrid

electrode with AM hydrosilylated pSi NPs, InP NCs and $Fe_2S_2(CO)_6$ catalyst, gave a 5.3 times higher photocurrent density at -1.6 µA/cm^2. When a -400 mV bias was applied to the hybrid electrode, an average photocurrent density of -2.1 µA/cm^2 was observed. The applied bias photo-to-current efficiency (ABPE) was calculated based on our previous work[15] and found to be 0.001%. Our system showed a 1.3 times increase in the photocurrent density for the hybrid pSi NPs electrode with applied bias when compared to the hybrid pSi NPs electrode without applied bias.

The charge transfer from pSi NPs (1.8 eV band gap) to InP NCs (1.35 eV band gap) and $Fe_2S_2(CO)_6$ (-0.9 eV band gap) catalyst under illumination assists H_2 production. The band gap alignment and charge transport mechanisms are analogous to our previous report using bulk pSi photocathode coated with InP NCs and $Fe_2S_2(CO)_6$ catalyst.[15]

Table 1. The photocurrent density measurements for the pSi NP decorated electrodes vs. Ag/AgCl reference electrodes in 0.1 M H_2SO_4 electrolyte.

Sample	Fabricated electrodes	OCPs	Photocurrent density (µA/cm^2)
A	AM-pSi NP on gold	-1.9 ± 1.6 mV	-0.3 ± 0.1
B	AM-pSi NPs + InP NCs + $Fe_2S_2(CO)_6$ catalyst on gold	-42.5 ± 60.1 mV	-1.6 ± 0.2
C	AM-pSi NPs + InP NCs + $Fe_2S_2(CO)_6$ catalyst on gold	-400.0 mV bias on -112.0 mV (sample B)	-2.1 ± 0.2

Fig. 3 shows the maximum current density measurements for the AM hydrosilylated pSi NPs on a gold electrode at 0 V and the OCP was measured to be -1.4 mV. The photocurrent density was found to be -300 nA/cm^2 and remained stable over several cycles. The inset shows the photographic image (A) and the SEM image (B) of the AM hydrosilylated pSi NPs assembled on a gold electrode.
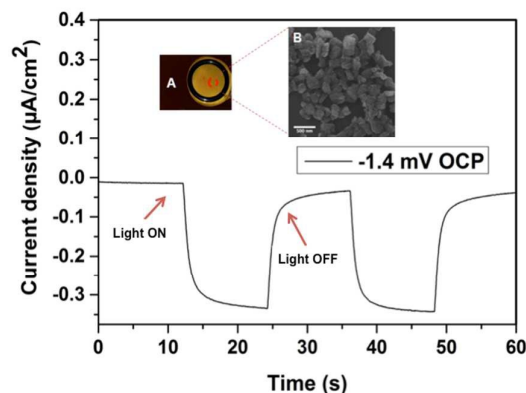

Fig. 3 The current density measurements for the AM hydrosilylated pSi NPs assembled on gold electrodes vs. Ag/AgCl reference

electrode in 0.1 M H_2SO_4 electrolyte. The inset A and B shows a photograph and a SEM image, respectively, of the pSi NPs assembled on a gold electrode.

Fig. 4 shows maximum current density measurements for the hybrid electrode at 0 V to -500 mV in steps of 100 mV. The bias potential of -500 mV showed a maximum photocurrent density of -6 $\mu A/cm^2$ with an OCP of -112 mV. However, a clear degradation of the photoelectrode was observed under these conditions. Therefore, we chose -400 mV bias potential which showed a stable performance with a maximum photocurrent density of -2.2 $\mu A/cm^2$. It is also clear that the bias did not affect the photocatalytic performance but just added an electrolytic component.

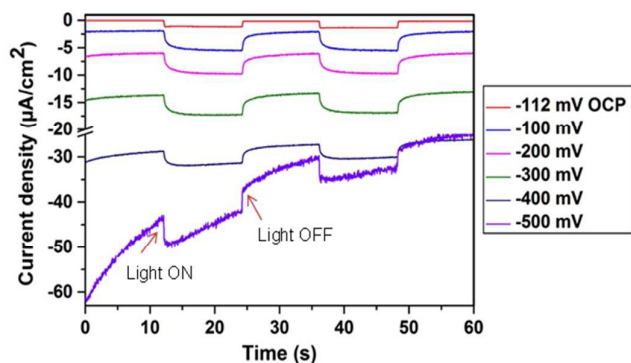**Fig. 4** The current density measurements for the hybrid electrode featuring pSi NPs, InP NCs + $Fe_2S_2(CO)_6$ catalyst vs. Ag/AgCl reference electrode in 0.1 M H_2SO_4 electrolyte. The current density was measured with steps of 100 mV of external bias with an OCP of -112 mV for every 12 s light/dark cycles.

Fig. 5 shows the 1 h current density measurements of the hybrid electrode at a bias potential of -400 mV vs. the OCP when the light was turned on; all other parameters of the photocurrent density measurements were kept constant. The current density trace dropped to -35 $\mu A/cm^2$ caused by the increase in the electrolytic activity. The current density slowly decreases with time due to the oxidation of pSi NPs in the slightly acidic electrolyte.[34] Unreacted Si-Hx groups remained after AM hydrosilylation on pSi NPs as evident from FTIR spectrum (Fig. 2b). The mechanism of oxidation involves the oxidative hydrolysis of unreacted Si-Hx groups to silicic acid.[35,36]
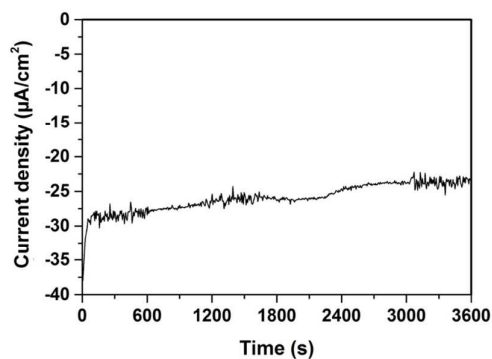

Fig. 5 The 1 h current density measurements for hybrid pSi NPs on a gold electrode vs. Ag/AgCl reference electrodes in 0.1 M H_2SO_4 electrolyte at a bias potential of -400 mV.

To measure the H_2 production, 310 µl of gas sample after 1 h was collected from the headspace of the PEC cell and analysed via GC. The peak at 0.533 min (Supporting Information, Fig. S3A) confirmed the presence of H_2.[37] Fig. S3B shows the result of GC analysis of 200 ppm of a H_2 standard. From the areas of the sample and standard H_2 peaks, the moles of H_2 produced were calculated to be approximately 5.84 nmol (see Supporting Information for calculation). Theoretically, a photocurrent density of -2.2 $\mu A/cm^2$ should produce 41 nmol of H_2 for 1 h of a water splitting reaction. However, the photocurrent density slightly decreased over time, suggesting that the stability of the system needs to be improved. Efforts to improve the stability through surface functionalisation of pSi NPs are currently in progress. The photocurrent density measured for hybrid pSi NPs electrode was less than for a bulk hybrid pSi electrode under identical conditions.[15] However, our hybrid pSi NPs electrode achieved a photocurrent density over twice as high as those compared to nanoporous silicon powder coated with tin dioxide.[25] We also demonstrated a strategy to fabricate a nanophotocathode using pSi NPs. This example can extend the application of pSi NPs for water splitting to other devices including solar cells and batteries.

Conclusions

We fabricated a PEC water-splitting electrode from *p*-type pSi NPs coupled with inexpensive inorganic nanomaterials, InP NCs and $Fe_2S_2(CO)_6$ catalyst. Our system achieved a photocurrent density of approximately -2.2 $\mu A/cm^2$ and 5.84 nmol of H_2/h was produced. This system provides a significant step forward into developing low cost PEC devices for renewable energy. Efforts focused on the use of various surface passivation techniques, such as thermal hydrocarbonisation and electrografting, to improve the stability of the pSi NPs photocathode system are underway.

Acknowledgements

Notes and references

1. T. Hisatomi, J. Kubota and K. Domen, *Chem. Soc. Rev.*, 2014, **43**, 7520-7535.
2. R. M. Navarro, F. del Valle, J. A. Villoria de la Mano, M. C. Álvarez Galván and J. L. G. Fierro, *Adv. Chem. Eng.*, 2009, **36**, 111-143.
3. R. M. Navarro Yerga, M. C. Álvarez Galván, F. del Valle, J. A. Villoria de la Mano and J. L. G. Fierro, *ChemSusChem*, 2009, **2**, 471-485.
4. A. Currao, *Chimia*, 2007, **61**,815-819.
5. T. Hisatomi, T. Minegishi and K. Domen, *Bull. Chem. Soc. Jpn.*, 2012, **85**, 647-655.
6. M. Matsuoka, M. Kitano, M. Takeuchi, K. Tsujimaru, M. Anpo and J. M. Thomas, *Catal. Today*, 2007, **122**, 51-61.
7. P. V. Kamat and D. Meisel, *Curr. Opin. Colloid Interface Sci.*, 2002, **7**, 282-287.
8. H. Bahruji, M. Bowker, P. R. Davies, L. S. Al-Mazroai, A. Dickinson, J. Greaves, D. James, L. Millard and F. Pedrono, *J. Photochem. Photobiol. A: Chem.*, 2010, **216**, 115-118.
9. A. Goetzberger, C. Hebling and H.-W. Schock, *Mater. Sci. Eng. R Rep.*, 2003, **40**, 1-46.
10. K. Sun, S. Shen, Y. Liang, P. E. Burrows, S. S. Mao and D. Wang, *Chem. Rev.*, 2014, **114**, 8662-8719.

RSC Advances Accepted Manuscript

11. Z. Qin, J. Joo, L. Gu and M. J. Sailor, *Part. Part. Syst. Char.*, 2014, **31**, 252-256.

12. T. J. Macdonald, Y. J. Mange, M. R. Dewi, H. U. Islam, I. P. Parkin, W. M. Skinner and T. Nann, *J. Mater. Chem. A*, 2015, **3**, 13324-13331.

13. L. Ji, M. D. McDaniel, S. Wang, A. B. Posadas, X. Li, H. Huang, J. C. Lee, A. A. Demkov, A. J. Bard, J. G. Ekerdt and E. T. Yu, *Nat. Nano*, 2015, **10**, 84-90.

14. B. Kumar, M. Beyler, C. P. Kubiak and S. Ott, *Chem. Eur. J.*, 2012, **18**, 1295-1298.

15. S. Chandrasekaran, T. J. Macdonald, Y. J. Mange, N. H. Voelcker and T. Nann, *J. Mater. Chem. A*, 2014, **2**, 9478-9481.

16. I. Oh, J. Kye and S. Hwang, *Bull. Korean Chem. Soc*, 2011, **32**, 4393.

17. I. Oh, J. Kye and S. Hwang, *Nano Letters*, 2011, **12**, 298-302.

18. K.-Q. Peng, X. Wang, X.-L. Wu and S.-T. Lee, *Nano Letters*, 2009, **9**, 3704-3709.

19. D. P. Tran, T. J. Macdonald, B. Wolfrum, R. Stockmann, T. Nann, A. Offenhäusser and B. Thierry, *Appl. Phys. Lett.*, 2014, **105**, 231116.

20. F. Erogbogbo, T. Lin, P. M. Tucciarone, K. M. LaJoie, L. Lai, G. D. Patki, P. N. Prasad and M. T. Swihart, *Nano Letters*, 2013, **13**, 451-456.

21. G. Bernhard, K. Dmitry and S. Olga, *Nanotechnology*, 2011, **22**, 305402.

22. P. Kale, A. C. Gangal, R. Edla and P. Sharma, *Int. J. Hydrogen Energy*, 2012, **37**, 3741-3747.

23. H. Bahruji, M. Bowker and P. R. Davies, *Int. J. Hydrogen Energy*, 2009, **34**, 8504-8510.

24. F. Dai, J. Zai, R. Yi, M. L. Gordin, H. Sohn, S. Chen and D. Wang, *Nat. Commun.*, 2014, **5**.

25. B. H. Meekins, Y.-C. Lin, J. S. Manser, K. Manukyan, A. S. Mukasyan, P. V. Kamat and P. J. McGinn, *ACS Appl. Mater. Interfaces*, 2013, **5**, 2943-2951.

26. T. Nann, S. K. Ibrahim, P.-M. Woi, S. Xu, J. Ziegler and C. J. Pickett, *Angew. Chem. Int. Ed.*, 2010, **49**, 1574-1577.

27. T. J. Macdonald and T. Nann, *Nanomaterials*, 2011, **1**, 79-88.

28. S. Chandrasekaran, M. J. Sweetman, K. Kant, W. Skinner, D. Losic, T. Nann and N. H. Voelcker, *Chem. Commun.*, 2014, **50**, 10441-10444.

29. S. Xu, J. Ziegler and T. Nann, *J. Mater. Chem.*, 2008, **18**, 2653-2656.

30. S. Xu, S. Kumar and T. Nann, *J. Am. Chem. Soc.*, 2006, **128**, 1054-1055.

31. J. Nelles, D. Sendor, A. Ebbers, F. Petrat, H. Wiggers, C. Schulz and U. Simon, *Colloid Polym. Sci.*, 2007, **285**, 729-736.

32. J. Nelles, D. Sendor, F.-M. Petrat and U. Simon, *J. Nanopart.Res.*, 2010, **12**, 1367-1375.

33. M. J. Sweetman, C. J. Shearer, J. G. Shapter and N. H. Voelcker, *Langmuir*, 2011, **27**, 9497-9503.

34. S. Chandrasekaran, T. J. Macdonald, A. R. Gerson, T. Nann, and N. H. Voelcker, *ACS Appl. Mater.Interfaces*, 2015, **7**, 17381–17387.

35. E.J. Anglin, L. Cheng, W.R. Freeman, M.J. Sailor, *Adv. Drug Del. Rev.,*2008*,* **60**, 1266-1277.

36. S.E. Letant, S. Content, T. T. Tan, F. Zenhausern and M.J. Sailor, *Sens. Actuator B-Chem.,* 2000, **69,** 193-198.

37. K. Zhang, D. Jing, C. Xing and L. Guo, *Int. J. Hydrogen Energy,* 2007, **32**, 4685-4691.

TOC
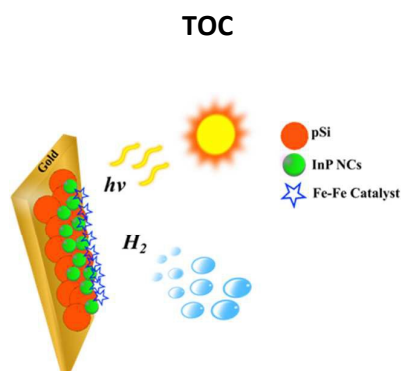
An investigation on the nanophotocathode fabrication using electrochemically anodised pSi NPs for photoelectrochemical water splitting.